The Structure of Ultrathin H-Passivated [112] Silicon Nanowires

Ning Lu
Department of Physics, Iowa State University, Ames, Iowa 50011

Cristian V. Ciobanu*
Division of Engineering, Colorado School of Mines, Golden, Colorado 80401

Tzu-Liang Chan
Institute for Computational Engineering and Science, University of Texas at Austin, Austin, Texas 78712

Feng-Chuan Chuang
Department of Physics, National Sun Yat-Sen University, Kaohsiung 804, Taiwan

Cai-Zhuang Wang and Kai-Ming Ho
U.S. Department of Energy Ames Laboratory and Physics Department, Iowa State University, Ames, Iowa 50011

Received: March 30, 2007

We report on the atomic structure and energetics of H-passivated silicon nanowires that are oriented along the [112] crystallographic direction and have effective diameters of approximately 1 nm and below. Using a genetic algorithm structural optimization followed by ab initio density functional theory calculations, we find that at certain values of the hydrogen chemical potential the nanowires can take relatively stable (magic) structures with rectangular cross sections bounded by monohydride {110} and {111} facets with dihydride wire edges. Variations in the chemical potential of hydrogen alter the wire structures retrieved by the optimization, the most prominent example of this being that the {111} nanofacets acquire trihydride terminations instead of monohydride ones when the H chemical potential is raised. While the trihydride-passivated wires have already been experimentally observed, the magic-number monohydride-facetted wires found here may serve as useful predictions to be tested in the future.

In recent years, the fundamental and technological efforts toward viable uses of nanostructures have markedly switched from carbon nanotubes to semiconductor nanowires, as the latter allow for a more diverse range of structures and, hopefully, for more control over their properties. Fervent strides are underway to synthesize nanoscale wires for nanoelectronics applications[1] because of the realization that such wires can operate both as nanoscale devices and as the leads that connect them.[2] Silicon nanowires (SiNWs) offer, in addition to their appeal as building blocks for nanoscale devices, the benefit of simple fabrication techniques compatible with the currently well-developed silicon technology.

Currently, the widely used methods of synthesis[3−6] can produce SiNWs with diameters ranging from several tens of nanometers down to 1 nm. The SiNWs are usually crystalline with a prismatic shape bounded by facets that are parallel to the axis of the wire.[4−8] While remarkable progress has been achieved on the front of synthesis and characterization, atomic-scale structural information remains necessary for a better understanding of the physics and potential applications of SiNWs. At small diameters, the resolution of scanning probing microscopy techniques may not be sufficient to unambiguously identify the positions of the atoms at the surface of the wire. Moreover, the current theoretical approaches do not routinely rely on exhaustive searches of the configuration space of nanowires for two reasons: (i) global search methodologies for quasi one-dimensional structures are not widely developed and used, and (ii) any global search method requires inexpensive ways to evaluate the energy of the system, which come in the form of empirical potentials. The empirical potentials may not always have sufficient accuracy to capture subtler wire configurations with similar energies and different structures. Therefore, numerous recent studies rely on heuristically proposed NW structures as a starting point for stability studies of SiNWs at the ab initio level.[9−14] Because the experimental techniques to date yield wires that are passivated either with oxides[15,16] or with hydrogen,[6,7] theoretical studies have recently started to address the structure and properties of hydrogenated nanowires.[17−23]

Experimental work by D.D.D. Ma et al.[6] has revealed that ultrathin nanowires with effective diameters[24] in the range of 1 to 7 nm can be produced by HF etching of the oxide sheath that covers the wire after the oxide-assisted growth procedure. Although the HF-etching process is initially dominated by kinetics, at the end of it the wire remains virtually free of surface defects and has facets with low-energy orientations. This observation has enabled us to simulate the formation of the ultrathin H-passivated [110] SiNWs through a process of minimization of the formation energy per atom, with results[23] that were strikingly close to the experimental ones.[6]

Here, we investigate the low-energy structures of hydrogenated ultrathin nanowires oriented along the [112] direction. We focus on the shape evolution of the cross-section as the number of Si atoms per length increases, and we also assess

* Corresponding author. E-mail: cciobanu@mines.edu. Phone: 303-384−2119. Fax: 303-273−3602.

10.1021/jp072519o CCC: $37.00
Published on Web 05/16/2007

the influence of the hydrogen environment on the cross-sectional shape. For hydrogen environments where monohydride terminations are favorable, we have found (via global configuration search) that the cross-sections of the stable or metastable wires are perfectly rectangular. However, the aspect ratio of the rectangles is not that given by the thermodynamic Wulff construction, which predicts that the distance from the wire axis to any given facet is strictly proportional to the surface energy of that facet orientation.[25] The structures corresponding to relatively deep local minima of the formation energy are called magic structures and are characterized by monohydride-facetted [112] wires with complete (111) bilayers. These magic NW structures have certain specific numbers of Si atoms, called magic numbers. When the number of Si atoms per wire length is increased, the length of the (111) bilayers grows first, before additional bilayers are formed. We have also found that variations in the chemical potential of hydrogen trigger changes in the wire shape and facet terminations, as well as in the relative energetics of the local minima of the formation energy per silicon atom.

To search for nanowire structures with low formation energies, we have employed a genetic algorithm (GA) because this methodology has proved to be versatile and efficient for a variety of silicon-based low-dimensional systems.[23,26] The SiNWs are modeled using a supercell that is periodic in one dimension with the periodic length along the wire set according to experimental reports.[6] We have chosen the Hansel−Vogl (HV) interatomic potential because the HV model reproduces well the energies of hydrogenated phases of the Si(001) surface.[27] The global optimization procedure has been recently put forth in ref 23, and we will only briefly describe it below.

During a GA optimization run, a pool of at least 60 structures is evolved by performing genetic operations (cross-overs). For this nanowire system, the crossover operation consists in randomly selecting two structures (parents) from the pool, cutting them with the same plane parallel to the wire axis, then combining parts of the parents that lie on the opposite sides on the cutting plane to create a new structure (child). The new structure is then fully passivated with H atoms and relaxed using the HV interatomic potential.[27] We include the child structure in the genetic pool based on its formation energy f, defined as

$$f = (E - \mu_H n_H)/n - \mu \qquad (1)$$

where E is the total energy of the supercell with n Si atoms and n_H hydrogen atoms, μ is the (reference) bulk cohesive energy of Si in the diamond phase, and μ_H is the chemical potential of hydrogen. The (variable) number of H atoms is determined by the requirement of having complete passivation of the wire surface, but n is kept fixed during the crossover operations by rejecting any child that has a different number of Si atoms than its parents.

The H chemical potential (μ_H) at the empirical interactions level[27] is chosen such that the experimentally relevant passivation reactions at surfaces are thermodynamically possible during the optimization. This means that μ_H is set such that certain hydrogenated surfaces have lower energies than the surface energies of the same orientations prior to the considered hydrogenation reaction. Guided by experiments,[6] we focus only on two surface orientations, Si(111) and Si(110), and determine the range of H chemical potentials for which the following reactions are thermodynamically allowed: (a) formation of monohydride Si(111) from clean, unreconstructed Si(111), (b) formation of monohydride Si(110) from clean Si(110), and (c) formation of trihydride Si(111) from monohydride Si(111). The ranges of allowable μ_H (at the HV level) for each of these three reactions are shown in Figure 1a. Within the μ_H range that is common to all three reactions, we choose two values (Figure 1a) that are close to the lower bound of μ_H, because this choice readily ensures (i) that the desired hydrogenation reactions are all allowed, and (ii) that the calculations are as far away as possible from the total etching regime in which the system could decompose in silane or disilane.

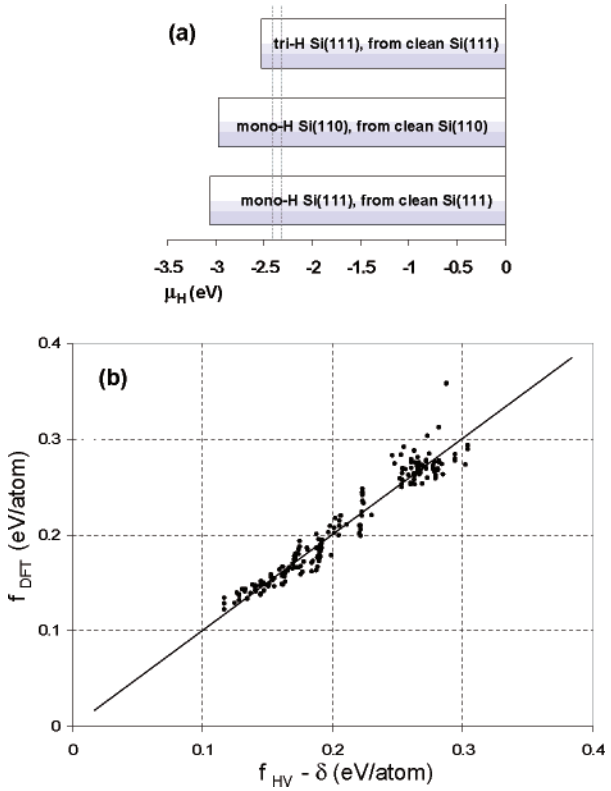

Figure 1. (a) Allowable HV chemical potential ranges for the three relevant hydrogenation reactions described in text. Two μ_H values ($\mu_H = -2.42$ eV and $\mu_H = -2.32$ eV, vertical dash lines) have been chosen close to the lower bound of the common μ_H range where all three passivation reactions are thermodynamically allowed. (b) DFT formation energies[28] (f_{DFT}) of 235 H-passivated [112] SiNWs plotted versus the HV formation energies corresponding to $\mu_H = -2.42$ eV. A least-squares fit yields $f_{DFT} = f_{HV} - \delta$ (where $\delta = 0.1$ eV/atom) for a DFT chemical potential of $\mu_H = -3.48$ eV.

The genetic pool is divided into two equal subsets, corresponding to the two chosen values μ_H (Figure 1a). The crossover operations are performed both with parents in the same subset and with parents in different subsets, to ensure a superior sampling of the potential energy landscape. The genetic operation is carried out 15 times during a generation, and a typical GA run has 50 000 generations. At the end of each run, all structures in the pool are relaxed using the VASP software;[28,29] this is a well-developed, broadly used package and, as such, it may ensure that the results presented here could be more widely reproduced. The chemical potential μ_H that we have used for computing the density functional theory (DFT) formation energies was determined by maximizing the correlation with the HV formation energies for 235 configurations of [112] H-passivated SiNWs [refer to Figure 1(b)]. A least-squares fit through the 235 data points yields the relation $f_{DFT} = f_{HV} - \delta$ between the formation energies at the DFT and HV levels, where $\delta = 0.1$ eV/atom. Because of this simple relationship, in Figure 1b we have shown the difference $f_{HV} - \delta$ on the horizontal axis, rather than showing f_{HV}. While some energetic reordering occurs upon performing the DFT calculations, most of the low-

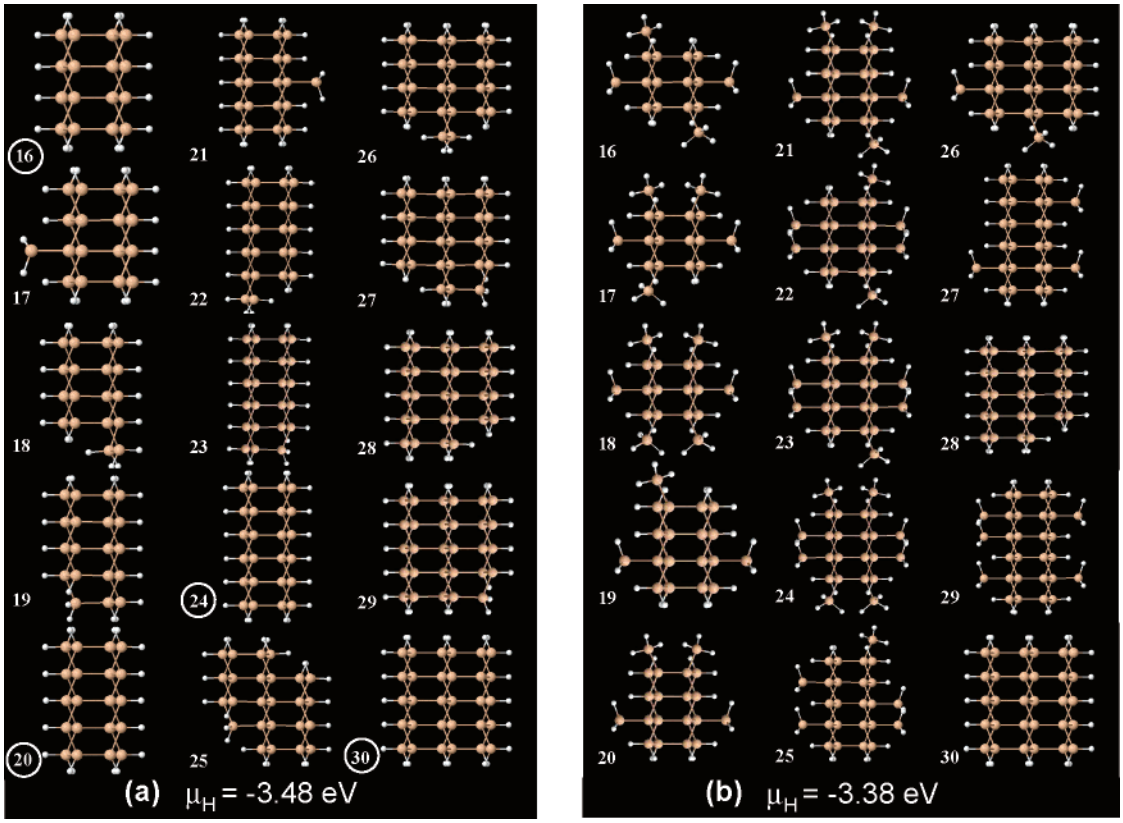

Figure 2. Nanowire structures (axial view along the [112] direction) with $n = 16-30$ silicon atoms per unit cell and H DFT chemical potential values of $\mu_H = -3.48$ eV (a) and $\mu_H = -3.38$ eV (b), found to have the lowest formation energy per atom (eq 1) after the genetic algorithm optimization and subsequent DFT relaxations. The H atoms are the smaller white spheres. The values n that correspond to magic nanowires (i.e., structures that correspond to pronounced local minima of the formation energy per atom) are circled.

energy structures found with the HV potential remain relevant at the DFT level, which gives confidence in the combined GA−DFT approach used here.

The structures found to have the lowest formation energy (eq 1) after the combined GA optimization and DFT relaxation are shown in Figure 2a,b for $16 \leq n \leq 30$ and for H chemical potentials of $\mu_H = -3.48$ and -3.38 eV, respectively. As can be seen in Figure 2, the two subsets of the genetic pool corresponding to the two H chemical potential values retrieved mostly different structures at each number n of Si atoms per unit cell. This result is markedly different from the one obtained for [110]-oriented nanowires,[23] where the best structures retrieved for even n values were the same for the small μ_H variation (0.1 eV) considered and where the odd-n structures differed only in the position of one peripheric atom.

At the lower chemical potential ($\mu_H = -3.48$ eV), the nanowires tend to have 90° edges whenever the number of atoms n allows, with the most stable wire having perfectly rectangular cross sections. For example, at $n = 16$ the atoms arrange themselves so that they form a rectangle with (111) facets that are longer than its (110) facets. The aspect ratio of the rectangle is not solely dictated by the ratio of surface energies as would be expected from the Wulff construction[25] but is strongly affected by the presence of dihydride corners and by the small number of atoms that prevents the formation of large (110) facets. As the number of atoms is increased, the extra atoms dispose themselves around the $n = 16$ core in such a way as to increase the length of the full (111) mono-H facets first (i.e., growth in the [110] direction). After $n = 24$, the wire also begins to grow along the [111] direction as the larger n can accommodate wider (110) facets to minimize the overall formation energy. The first perfect rectangle with more than two (111) planes (complete bilayer structures) appears at $n = 30$, as seen in Figure 2a.

For the larger H chemical potential ($\mu_H = -3.38$ eV), there is no clear preferential growth pattern, and we have not found any particularly stable structures. At this chemical potential, there are more trihydride species on the wires leading to a variety of floppy structures (e.g., the surface of the nanowire with $n = 18$). The existence of many such structures with very similar energies prevents the emergence of a systematic or clear evolution pattern of the cross section of the wire. While in Figure 2a for $n > 24$ the wires tend to form three complete (111) bilayers with mono-H coverage, in the case of $\mu_H = -3.38$ eV (Figure 2b) the (111) facets are covered by a mixture of trihydrides and monohydrides that results in a variety of NW structures that have incomplete (111) layers.

The formation energy f of the most stable structures that we found for $16 \leq n \leq 30$ is plotted in Figure 3 as a function of n. When trihydrides are strongly disfavored ($\mu_H = -3.48$ eV), the formation energy displays clear local minima at $n = 16$, 20, 24, and 30 with the structures identified in Figure 2a. These local minima structures have rectangular cross-sections, are fully covered in monohydrides, and their facet edges consist of dihydrides (SiH_2). Because of their relatively low-formation energies, we may call these structures magic nanowires. In the ultrathin regime, the aspect ratio of the cross-section of the magic wires does not vary monotonically (as can be seen by inspecting Figure 2a) but settles at the value predicted by the surface energy ratio[25] in the limit of a very large number of atoms n (i.e., for thick nanowires). At the higher value of μ_H, the formation energy does not display pronounced local minima (Figure 3). The two minima located at $n = 21$ and $n = 27$ do not have symmetric structures, and they are not deep minima

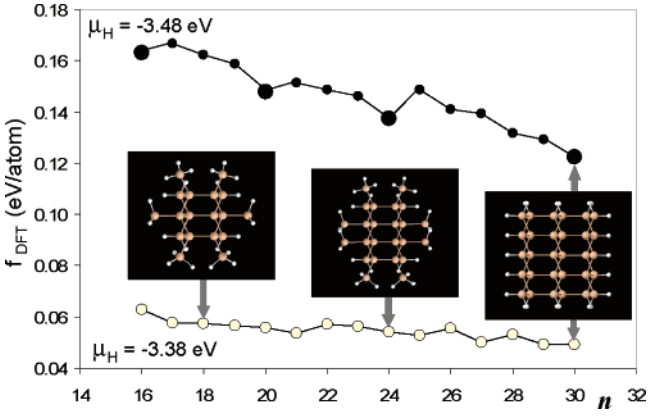

Figure 3. DFT formation energies for two values of the H chemical potential $\mu_H = -3.48$ eV (solid dots) and $\mu_H = -3.38$ eV (open circles), plotted as a function of the number n of Si atoms. When mostly monohydrides cover the nanowire surface, the formation energy displays several pronounced local minima (large solid dots on the $\mu_H = -3.48$ eV curve) at $n = 16$, 20, 24, and 30 (magic numbers). If a significant amount of trihydrides are formed (which happens for $\mu_H = -3.38$ eV), then deep minima of the formation energies do not occur; in this case, the much smaller variations of the formation energy are due to a large number of competing configurations with both mono- and trihydrides on the surface. The insets show that even structures with clear spatial symmetry do not give local minima on the $\mu_H = -3.38$ eV formation energy curve.

either. The $\mu_H = -3.38$ eV structures displayed as insets at $n = 18$, 24, and 30 are symmetric but are not local minima (Figure 3).

We have therefore evidenced that a (slight) change in μ_H can have a large effect on the wire structure in that it can determine whether magic structures could be identified or not. The higher H chemical potential ($\mu_H = -3.38$ eV) does not yield magic structures because the trihydrides on the (111) facets are able to relax in the vicinity of monohydrides and dihydride edges, thus allowing for numerous low-energy combinations of SiH_x species on the wire surface. In contrast, for $\mu_H = -3.48$ eV the surface energy of the tri-H/Si(111) surface is very high (more than twice the value corresponding to mono-H/Si(111) surfaces) because of the larger absolute value of the chemical potential and irrespective of the relaxation of the trihydrides. By this reasoning, we should be able to tune μ_H to values that render the monohydride (111) surfaces completely unfavorable. We tested μ_H values of -3.28 eV and higher and have found that the trihydrides indeed become the preferred species on the (111) wire facets.

The above discussion has focused on whether or not we can observe magic nanowires for different chemical potentials μ_H, and we identifyed rectangular wires with (110) and (111) facets. The (111) facets can be covered by mono or trihydrides for the most favorable structures at $\mu_H = -3.48$ and -3.28 eV, respectively. These types of wires have simple geometries, characterized by the number of N of (110) layers and the number M of complete (111) bilayers (Figure 4). In the trihydride case, there are $(M - 1)$ complete bilayers inside the wire plus one-half of a bilayer on each of the two (111) facets that bound the wire and are subject to passivation (Figure 4b). The total number of Si atoms and the number of hydrides of each kind for rectangular nanowires made of complete bilayers are summarized in Table 1.

In the recent experiments[6] on H-passivated [112] SiNWs with diameters of ~2 nm, the (111) facets are passivated with trihydrides, which correspond to low-energy structures found for chemical potentials μ_H greater than -3.28 eV in our

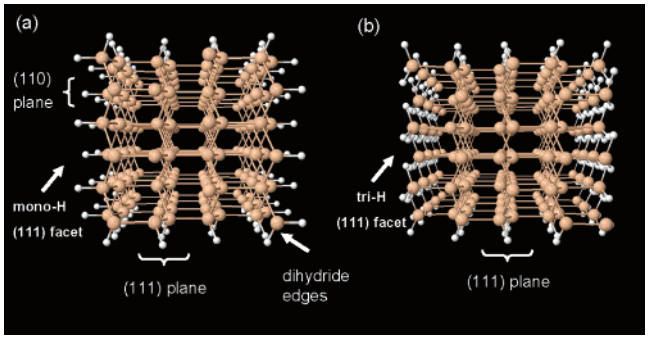

Figure 4. Perspective view along the axis of [112] H-passivated Si nanowires with monohydride (a) and trihydride (b) (111) facets. The (110)-type facets are covered with monohydrides in both cases. The nanowires shown (a,b) correspond to $N = 6$ planes parallel to (110), and $M = 4$ complete (111) bilayers. The trihydride-terminated wire (b) has one-half of a complete bilayer on each of the two (111) nanofacets. Structures of the type (a) have been identified as magic (refer to text and to Figures 2 and 3).

TABLE 1: Constituents of the [112] Hydrogenated Si Nanowires with Perfectly Rectangular Cross Sections Made of *N* (110)-oriented Planes and *M* (111) Planes (complete Bilayers).

structure	Si atoms, n	mono-H	di-H	tri-H
Figure 4a	$2NM$	$2(N + M - 2)$	4	0
Figure 4b	$2NM$	$2(M - 1)$	0	$2N$

simulations (refer to Figure 4b and Table 1). To our knowledge, passivated [112] SiNWs that have monohydride (111) facets have not been reported so far. The results of the global optimization presented here (Figures 2 and 3) indicate that the magic structures with mono-H/Si(111) should be experimentally observable, perhaps under different conditions than those reported in ref 6. The pioneering work of Higashi et al.[31] in the field of aqueous HF etching of silicon surfaces reported perfect mono-H coverage of Si(111) wafers, thus lending strong support to the above prediction of monohydride-facetted [112] nanowires.

In the diameter regime addressed here, the surface passivation (mono versus trihydride) can very likely have a strong effect on the electronic properties, because the number of atoms that are passivated is relatively large. The actual trends exhibited by structure, stability, band gap, and conductivity of [112] H-SiNWs as functions of the degree of hydrogenation are yet to be explored, as is the sensitivity of these trends with respect to possible random defects (vacancies) in the mono or trihydride coverage pattern. At equal areal density of missing hydrogen atoms, we would naturally expect the monohydride-terminated surfaces to be more sensitive to the presence of H-vacancies because a missing H atom in a monohydride-terminated wire generates a highly reactive Si site on the surface. Finally, we note that low levels of the H coverage can determine surface reconstructions (Si−Si bonding), whose energetics are determined, at least in certain μ_H regimes, by the number of passivated bonds per surface area.[32]

An interesting issue to address is whether one can create experimentally wires with a preset or controlled aspect ratio of the cross-section. The reason why this might be of interest is that in the ultrathin diameter regime where most of the atoms are at the surface, the interplay between the relative numbers of atoms on the (111) and (110) surfaces and their degree of H-passivation is likely to result in new (and perhaps useful) ways to control the band structure and optical properties of the nanowires. For example, the extent of band gap and band structure variations with the aspect ratio taken (at constant

effective wire diameter) is still unknown and is likely be addressed in the near future. If experimental conditions could be achieved so as to favor thermodynamics over the kinetics of the H-passivation process, the results presented here indicate that in such conditions the aspect ratios of the [112] Si NWs are determined only by the number of silicon atoms per unit length (cross-sectional area) and the effective H chemical potential attained in experimental conditions. On the other hand, because thermodynamics is not the only factor influencing the wire formation process we may expect to see broad distributions of aspect ratios, possibly with frequency distribution peaks located at ratios that correspond to the magic structures shown in Figure 2a. Because the few reported statistics on nanowires concern the effective wire diameters in relation to their growth direction[7,8] but do not address the aspect ratio, we believe it would be very interesting to pursue studies that can shed more light on the aspect ratio distributions of ultrathin hydrogenated nanowires of different diameters and axis orientations.

Acknowledgment. Ames Laboratory is operated for the U.S. Department of Energy by Iowa State University under Contract No. W-7405-Eng-82. This work was supported by the Director for Energy Research, Office of Basic Energy Sciences. We gratefully acknowledge grants of supercomputer time from NERSC in Berkeley and from NCSA Urbana−Champaign (DMR-050031).

References and Notes

(1) Appell, D. *Nature* (London) **2002**, *419*, 553.
(2) Cui Y.; Lieber, C. M. *Science* **2001**, *291*, 851.
(3) Morales A. M.; Lieber, C. M. *Science* **1998**, *269*, 208.
(4) Zhang, R. Q.; Lifshitz, Y.; Lee, S. T. *Adv. Mater.* **2003**, *15*, 635.
(5) Holmes, J. D.; Johnston, K. P.; Doty, R. C.; Korgel, B. A. *Science* **2000**, *287*, 1471.
(6) Ma, D. D. D.; Lee, C. S.; Au, F. C. K.; Tong, S. Y.; Lee, S. T. *Science* **2003**, *299*, 1874.
(7) Wu, Y.; Cui, Y.; Huynh, L.; Barrelet, C. J.; Bell, D. C.; Lieber, C. M. *Nano Lett*. **2004**, *4*, 433.
(8) Schmidt, V.; Senz, S.; and Gösele, U. *Nano Lett.* **2005**, *5*, 931.
(9) Menon M.; and Richter, E. *Phys. Rev. Lett.* **1999**, *83*, 792.
(10) Zhao Y.; Yakobson, B. I. *Phys. Rev. Lett.* **2003**, *91*, 035501.
(11) Bai, J.; Zeng, X. C.; Tanaka, H.; Zeng, J. Y. *Proc. Natl. Acad. Sci. U.S.A.* **2004**, *101*, 2664.
(12) Rurali R.; Lorente, N. *Phys. Rev. Lett.* **2005**, *94*, 026805.
(13) Kagimura, R.; Nunes, R. W.; Chacham, H. *Phys. Rev. Lett.* **2005**, *95*, 115502.
(14) Cao, J. X.; Gong, X. G.; Zhong, J. Z.; Wu, R. Q. *Phys. Rev. Lett.* **2006**, *97*, 136105.
(15) Cui, Y.; Gudiksen, L. J.; Wang, M. S.; Lieber, C. M. *Appl. Phys. Lett*. **2001**, *78*, 2214.
(16) Wang, N.; Tang, Y. H.; Zhang, Y. F.; Lee, C. S.; Bello, I.; Lee, S. T. *Chem. Phys. Lett.* **1999**, *299*, 237.
(17) Zhang, R. Q.; Lifshitz, Y.; Ma, D. D. D.; Zhao, Y. L. Frauenheim, Th.; Lee, S. T.; Tong, S. Y. *J. Chem. Phys.* **2005**, *123*, 144703.
(18) Beckman, S. P.; Han, J. X.; Chelikowsky, J. R. *Phys. Rev. B* **2006,** *74*, 165314.
(19) Singh, A. K.; Kumar, V.; Note, R.; Kawazoe, Y. *Nano Lett.* **2006**, *6*, 920.
(20) Tang Z.; Aluru, N. R. *Phys. Rev. B* **2006**, *74*, 235441.
(21) Jing, M. W.; Ni, M.; Song, W.; Lu, J.; Gao, Z. X.; Lai, L.; Mei, W. N.; Yu, D. P.; Ye, H. Q.; Wang, L. *J. Phys. Chem. B* **2006**, *110*, 18332.
(22) Zhao, X.; Wei, C. M.; Yang, L.; Chou, M. Y. *Phys. Rev. Lett*. **2004**, *92*, 236805.
(23) Chan, T. L.; Ciobanu, C. V.; Chuang, F. C.; Lu, N.; Wang, C. Z.; Ho, K. M. *Nano Lett.* **2006**, *6*, 277.
(24) The effective diameter is defined here as the diameter of the thinnest cylinder that includes all the silicon atoms of the wire.
(25) Pimpinelli A.; Villain, J. *Physics of Crystal Growth*; Cambridge University Press: New York, 1998; Chapter 3.
(26) (a) Ho, K. M.; Shvartsburg, A. A.; Pan, B. C.; Lu, Z. Y.; Wang, C. Z.; Wacker, J.; Fye, J. L.; Jarrold, M. F. *Nature* **1998**, *392*, 582. (b) Chuang, F. C.; Ciobanu, C. V.; Shenoy, V. B.; Wang, C. Z.; Ho, K. M. *Surf. Sci.* **2004**, *573*, L375. (c) Ge, Y. B.; Head, J. D. *J. Phys. Chem. B.* **2004**, *108*, 6025. (d) Chakraborty, N.; Prasad, R. *Bull. Mater. Sci.* **2003**, *26*, 127.
(27) Hansen U.; Vogl, P. *Phys. Rev. B* **1998,** *57*, 13295.
(28) (a) VIENNA ab initio simulation package (VASP); Universität Wien, 1999. (b) Kresse G.; Hafner, J. *Phys. Rev. B* **1993**, *47*, R558. (c) Kresse G.; Furthmüller, J. *Phys. Rev. B* **1996**, *54*, 11169.
(29) The ab initio calculations are performed within the generalized gradient approximation.[30] The kinetic energy cutoff is set at 11 Ry, and the Brillouin zone is sampled using 16 *k*-points. The SiNW is positioned at the center of a supercell with a vacuum space of 12 Å separating the periodic images of the wires. Each SiNW structure is relaxed until the magnitude of the force an any atom is smaller than 0.01 eV/Å.
(30) Perdew, J. P. In *Electronic Structure of Solids '91*; Ziesche, P., Eschrig, H., Eds.; Akademie-Verlag: Berlin, 1991.
(31) Higashi, G. S.; Chabal, Y. J.; Trucks, G. W.; and Raghavachari, K. *Appl. Phys. Lett.* **1990,** *56*, 656**.**
(32) Ciobanu C. V.; and Briggs, R. M. *Appl. Phys. Lett.* **2006,** *88*, 133125**.**